Ultrasonic Imaging 3, 37-61 (1981)

TRANSIENT FIELDS OF CONCAVE ANNULAR ARRAYS

Marcel Arditi, F. Stuart Foster, and John W. Hunt

The Ontario Cancer Institute and
Department of Medical Biophysics
University of Toronto
500 Sherbourne Street
Toronto, Canada M4X 1K9

A new analytic expression for the impulse response of concave radiators is used to compute the transient pressure distributions of phased annular arrays with spherical geometry. The process of phasing the array to achieve variable focusing is treated by summing the delayed impulse responses of the individual annuli. The example of pressure distributions of a five element annular array is treated in detail, and some recommendations are given for practical computer studies.

Key words: Annular array; concave; field; focused; impulse response; spherical; transient; ultrasound.

I. INTRODUCTION

Because the lateral resolution of medical echographical scanners depends primarily on the ultrasonic beam width, focused transducers are often used in these instruments to concentrate the acoustic energy in a focal region. This is commonly achieved by means of an acoustic lens, or by the use of concave spherically shaped radiators, methods that we shall refer to as "geometric" focusing.

The first reference to the use of a focused ultrasonic generator was made by Gruetzmacher in 1935 [1]. He achieved high ultrasound intensities at the centre of curvature of a large, spherically ground piezoelectric crystal, in the cw excitation mode. In 1945, Labaw [2] investigated the pressure fields of weakly focused transducers, but it was not until 1949 that O'Neil [3] published a rigorous theoretical analysis of the spherical source geometry. He derived the cw pressure distribution of uniformly excited focused radiators for observation points on the axis of symmetry or near the focal plane.

When ultrasound transducers are excited by short electrical pulses as is common in medical scanners, their transient pressure fields are given by a superposition of a wide spectrum of frequencies. In this case, field calculations are most efficiently performed by convolution of the driving waveform with the source's impulse response, as described, for example, by Stepanishen [5].

The theoretical treatment of short pulse propagation from plane pistons has been given great attention. In 1960, Oberhettinger [4] first derived an analytic expression of the impulse response for this geometry, and since then many interesting papers have been published on the transient radiation patterns from baffled plane pistons with circular or rectangular boundaries [5-8]. However, the case of pulsed focused

0161-7346/81/010037-25$02.00/0

radiators has received comparatively little attention [9,10]. The design of weakly focused transducers has been discussed by Kossoff [11], who also described, from a geometric point of view, their axial transient responses.

An analytic solution of the impulse response of spherical radiators was found in 1976 by Penttinen and Luukkala [12]. Although these authors did not discuss pulsed excitation, their analytic impulse response can be directly used for theoretical calculations of transient fields, providing an elegant approach to this problem.

Because of the reduced depth of field characteristic of strongly focused apertures, the use of phased, electronically focused annular arrays with rapidly variable focal lengths was suggested as early as 1956 by Reid and Wild [13]. The idea was to provide large effective depth of field without compromising lateral resolution. Although the first approaches only considered plane arrays (e.g.[14]), simplified electronics design was later reported [15-17] when variable electronic focusing was used in conjunction with geometric focusing at a preselected depth. Recently, Dietz et al. [18,19] analyzed the wideband response of plane annular arrays. They treated the aperture as an array of infinitely thin annular elements; using an approximate expression of the impulse response of thin annuli, they studied the array focal plane response and reported good agreement with experimental results.

In this paper, we present a theoretical treatment of pulsed annular arrays with geometric focusing. A new compact formulation of the impulse response of spherical elements is given. The cases of a single element, an annular shell, and an annular array are treated successively. Finally, as an example, the pressure distribution from a strongly focused, five element annular array is treated in detail.

II SUMMARY OF THEORY

By reciprocity of sound wave propagation, pressure distributions from a transmitting radiator also describe its spatial sensitivity in the receiving mode. For convenience, we shall consider the radiator as a transmitter. From the classical theory of sound [20], the instantaneous pressure $p(\vec{r},t)$ at a point $P(\vec{r})$ and time t in the field of an ultrasound source can be expressed as

$$p(\vec{r},t) = -\rho \frac{\partial \phi}{\partial t}(\vec{r},t) \quad , \tag{1}$$

where ρ is the equilibrium density of the medium, and $\phi(\vec{r},t)$ is the velocity potential. For the case of a uniformly excited planar radiator of area S in an infinite baffle, $\phi(\vec{r},t)$ is given by:

$$\phi(\vec{r},t) = \frac{1}{2\pi} \int_S \frac{v_o(t - r'/c)}{r'} \, dS \quad , \tag{2}$$

where $v_o(t)$ is the instantaneous normal particle velocity at the face of the source. As illustrated in figure 1, r' is the distance separating

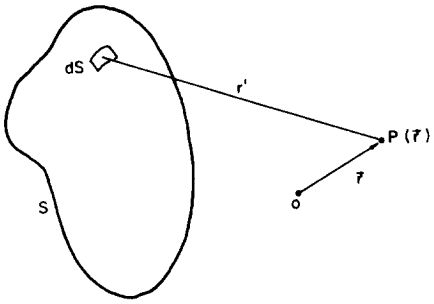

Fig. 1. Geometry used in Eq. (2).

the field point P from the integration surface element dS, and c is the speed of sound. The validity of Eq. (2) is limited to regions in which the obliquity factor can be ignored [21]. Further, we assume linear propagation in a non-attenuating, homogeneous medium.

When the source is not plane, but convex as is common in medical ultrasound transducers, the wave radiated by the source is diffracted by its own surface. This secondary radiation contributes theoretically to the pressure field but is not taken into account by Eq. (2). However, as noted by O'Neil [3] and Penttinen and Luukkala [12], Eq. (2) can be used as an excellent approximation for most practical applications, where the diameter of the source is large compared to the ultrasound wavelength, and the source only slightly curved. Under these conditions, the integral in Eq. (2) has to be evaluated over the spherical concave surface of the source.

As discussed in previous articles [5-8], Eq. (2) may be rewritten as

$$\phi(\vec{r},t) = v_o(t) * h(\vec{r},t) \quad , \tag{3}$$

where * is the convolution product in the time domain, and $h(\vec{r},t)$, called the impulse response of the source, is defined by

$$h(\vec{r},t) = \frac{1}{2\pi} \int_S \frac{\delta(t - r'/c)}{r'} \, dS \quad . \tag{4}$$

Note that the impulse response contains all the amplitude and phase information necessary to calculate the pressure field. Comparing Eq. (4) with Eq. (2), $h(\vec{r},t)$ may be considered as the velocity potential in the field of a source generating a velocity impulse at its face. The actual velocity potential for an arbitrary excitation is then evaluated using Eq. (3). The substitution of the time derivative of $\phi(\vec{r},t)$ into Eq. (1) then yields:

$$p(\vec{r},t) = - \rho \frac{\partial v_o}{\partial t} * h(\vec{r},t) \quad . \tag{5}$$

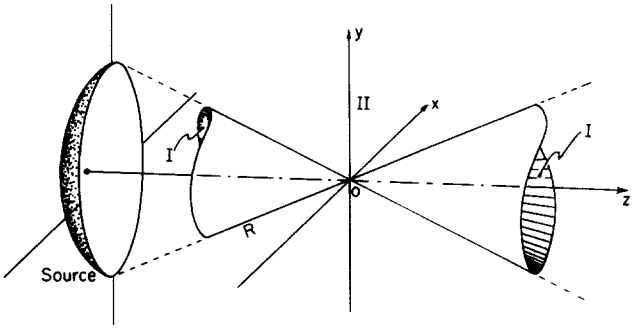

Fig. 2. Two separate regions, I and II, are used to describe the impulse response of a focused source.

Because $h(\vec{r},t)$ is determined by the source geometry only, Eq. (5) provides great flexibility for demonstrating the effects of various pulse shapes on the pressure fields of a given source. Furthermore, analytic expressions for $h(\vec{r},t)$ have been derived for several geometries [4,7,12]. In these cases, the instantaneous pressure for pulsed excitation can be calculated by a single numerical integration of Eq. (5), rather than performing the double integral of Eq. (2). Since the spherical source geometry can be treated analytically, transient pressure fields from concave annular arrays are therefore most efficiently studied by the impulse response approach.

III. IMPULSE RESPONSE OF CONCAVE SPHERICAL RADIATORS

In this section, we introduce a new formulation of the analytic solution for the impulse response of concave spherical radiators. The basic properties of this function are first discussed, then applied to the cases of annuli and arrays of phased concentric annular elements.

a) Single concave spherical shell

A description of $h(\vec{r},t)$ for this geometry is given in [12], where an analytic solution to the integral of Eq. (2) was found. For our study of concave annular arrays, we preferred to use a simpler and more compact form of the solution. The exact derivation of this new formulation is given in Appendix A.

To express the solution, it is convenient to divide the half space in front of the source into two regions, I and II, as indicated in figure 2, with the origin at the center of curvature of the concave radiator. Region I comprises the field inside the double cone subtended by the circular boundary of the aperture and its centre of curvature. Region II is defined as the rest of the field in front of the source. Because of the symmetry around the axis of the radiator, the description of $h(\vec{r},t)$ in the field can be restricted to the (y,z) plane with $y > o$. Polar coordinates ($r=|\vec{r}|, \theta$) are used in that plane, related to the rectangular system by

$$y = r \sin\theta \quad , \quad z = r \cos\theta \quad . \tag{6}$$

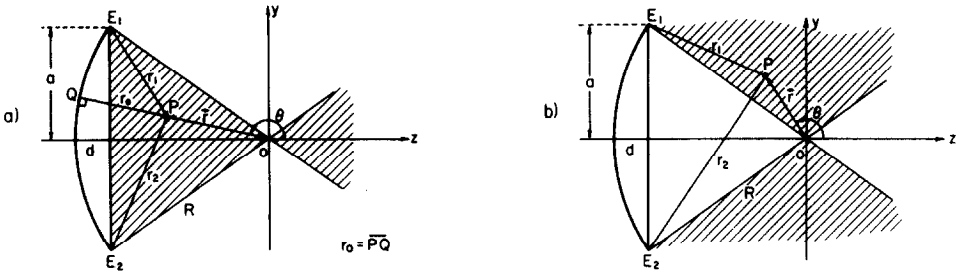

Fig. 3. a) Illustration of the quantities r_o, r_1, and r_2 for observation points P in Region I (shaded).

b) Illustration of r_1 and r_2 for P in Region II (shaded).

Figures 3(a) and 3(b) illustrate some quantities needed to express the solution, for Regions I and II respectively. The depth d of the concave source is given by the exact relationship:

$$d = R \{ 1 - (1 - \frac{a^2}{R^2})^{1/2} \} \quad , \tag{7}$$

where R is the radius of curvature of the source, and a the radius of its circular boundary. For field points P in Region I, r_o is defined as the shortest (for $z < o$) or longest (for $z > o$) distance between P and the source, and is given by:

$$r_o = \begin{cases} R - r & \text{for } z < 0 \\ R + r & \text{for } z > 0 \end{cases} \quad . \tag{8}$$

For both Regions I and II, r_1 and r_2 represent the distances from P to the closest and furthest edges (E_1 and E_2 respectively) of the radiator. They can be expressed more simply in rectangular coordinates:

$$\begin{aligned} r_1 &= \{ (a - y)^2 + (R - d + z)^2 \}^{1/2} \\ r_2 &= \{ (a + y)^2 + (R - d + z)^2 \}^{1/2} \quad . \end{aligned} \tag{9}$$

The above quantities having been defined, the analytic solution can now be expressed as a function of time and position. The result derived in Appendix A is given in full in table I for both Regions I and II.

The validity of table I is governed by that of Eq. (2). Therefore, pressure distributions can be accurately predicted throughout the field of the radiator. By treating the special case of a radiator

Table I. Impulse response $h(\vec{r},t)$ of a concave spherical radiator. The quantities r_o, r_1, and r_2 are defined in the text and figure 3.

$$h(\vec{r},t) = \begin{cases} 0 & \text{Region I: } z<0,\ ct<r_0 \quad \text{Region I: } z>0,\ r_0<ct \quad \text{Region II: } ct<r_1 \\ \dfrac{cR}{r} & \text{Region I: } z<0,\ r_0<ct<r_1 \quad \text{Region I: } z>0,\ r_2<ct<r_0 \quad \text{Region II: } - \\ \dfrac{cR}{r}\,\dfrac{1}{\pi}\cos^{-1}\left[\dfrac{\eta(t)}{\sigma(t)}\right] & \text{Region I: } z<0,\ r_1<ct<r_2 \quad \text{Region I: } z>0,\ r_1<ct<r_2 \quad \text{Region II: } r_1<ct<r_2 \\ 0 & \text{Region I: } z<0,\ r_2<ct \quad \text{Region I: } z>0,\ ct<r_1 \quad \text{Region II: } r_2<ct \end{cases}$$

with:

$$\eta(t) = R\left\{\frac{1-d/R}{\sin\theta} + \frac{1}{\tan\theta}\left(\frac{R^2+r^2-c^2t^2}{2rR}\right)\right\}$$

$$\sigma(t) = R\left\{1 - \left(\frac{R^2+r^2-c^2t^2}{2rR}\right)^2\right\}^{1/2}$$

focused at infinity, it is possible to derive from table I the well-established expressions for the impulse response of a plane piston [4].

Without going into a detailed description of the behavior of $h(\vec{r},t)$, we briefly examine here its main features.

i) On the axis ($y = o$). In this case, the entire circular boundary is equidistant from P, and the distances r_1 and r_2 from Eq. (9) are identical. Therefore, the single non zero portion of $h(\vec{r},t)$ as given in table I is a constant equal to $cR/|z|$, defined in a time interval bound by the first and last arrival from the source. Using the "rectangle" function defined in [21] as

$$\text{rect}(\xi) = \begin{cases} 1 & \text{for } -1/2 < \xi < 1/2 \\ 0 & \text{otherwise} \end{cases}, \tag{10}$$

the impulse response becomes

$$h(z,t) = \frac{c\,R}{|z|}\,\text{rect}\left(\frac{ct - M}{\Delta(z)}\right), \tag{11}$$

where M is the mean distance $(r_o + r_1)/2$ and $\Delta(z)$ the path difference $(r_1 - r_o)$.

ii) At the centre of curvature ($y = z = o$). Here the amplitude of $h(\vec{r},t)$ goes to infinity, whereas its interval of definition tends to zero. More precisely, one can show that for the limit $z \to 0$, the integral of Eq. (11) over the interval of definition of $h(\vec{r},t)$ is equal

to the depth d of the concave radiator. The impulse response at the focus may therefore be written as

$$h(0,t) = d\,\delta(t - R/c) \quad , \tag{12}$$

according to the definition of the δ-function. From Eq. (5), the pressure waveform at this point is a replica of the time derivative of the normal velocity at the face of the source.

iii) Off the axis of symmetry ($y > o$). In this case, the behavior of $h(\vec{r},t)$ can best be described with the help of figure 4, which shows three-dimensional plots of the impulse response in the field of a focused transducer with $R/a = 4.8$. Three cross sections are examined, at the following depths: a) $z = -R/6$, b) $z = 0$ (focal plane), and c) $z = +R/4$. At observation points in front of the focal plane [a), $z < 0$], a qualitative resemblance with the case of a plane piston can be observed (e.g. [7]). In Region I (geometric projection of the source), h has first a constant value, which lasts from the first arrival time from the source (r_o/c) until the arrival from the closest edge E_1 (r_1/c). Note that, in contrast with the plane piston case, the value cR/r of this constant portion varies with position. Then, between the times r_1/c and r_2/c (contribution from the furthest edge E_2), $h(\vec{r},t)$ decreases monotonically to zero. In Region II, it varies continuously between r_1/c and r_2/c. In the focal plane [b), $z = 0$], the constant portion never exists, because the first and last arrivals are always contributions from the edges E_1 and E_2. Behind the focal plane [c), $z > 0$], the similarity with the case $z < 0$ can be noted, with a reversal in the succession of contributions from the source, already mentioned by Penttinen and Luukkala [12].

b) Single concave annulus

We shall now examine the case of a single concave annulus. An understanding of this geometry is a necessary preliminary to the treatment of phased annular arrays. The geometry of the single concave annulus is shown in figure 5. The inner and outer radii a_1 and a_2 of the annulus form the outer radii of 2 spherical surfaces, S_1 and S_2. The spherical surface S_a of the annulus is considered as the difference between S_1 and S_2 and it is possible to write the impulse response of the annulus as the difference between the impulse responses of the spherical surfaces. Thus:

$$h_a(\vec{r},t) = h_2(\vec{r},t) - h_1(\vec{r},t) \quad , \tag{13}$$

where h_a refers to the annulus, and h_1 and h_2 refer to the surfaces S_1 and S_2 respectively.

Because h_1 and h_2 are impulse responses of spherical radiators, the analytic solution given in table I may be used to determine the pressure distribution of the focused annulus. However, care must be taken to consider the cases of h_1 and h_2 separately, since certain field points may lie inside Region I of S_2 and Region II of S_1 simultaneously. The impulse response could then have up to five breakpoints as a function of time: The first arrival from inside the annulus, and, in general, four arrivals from the edges of the annulus. Although it would be tedious to formulate the complete mathematical

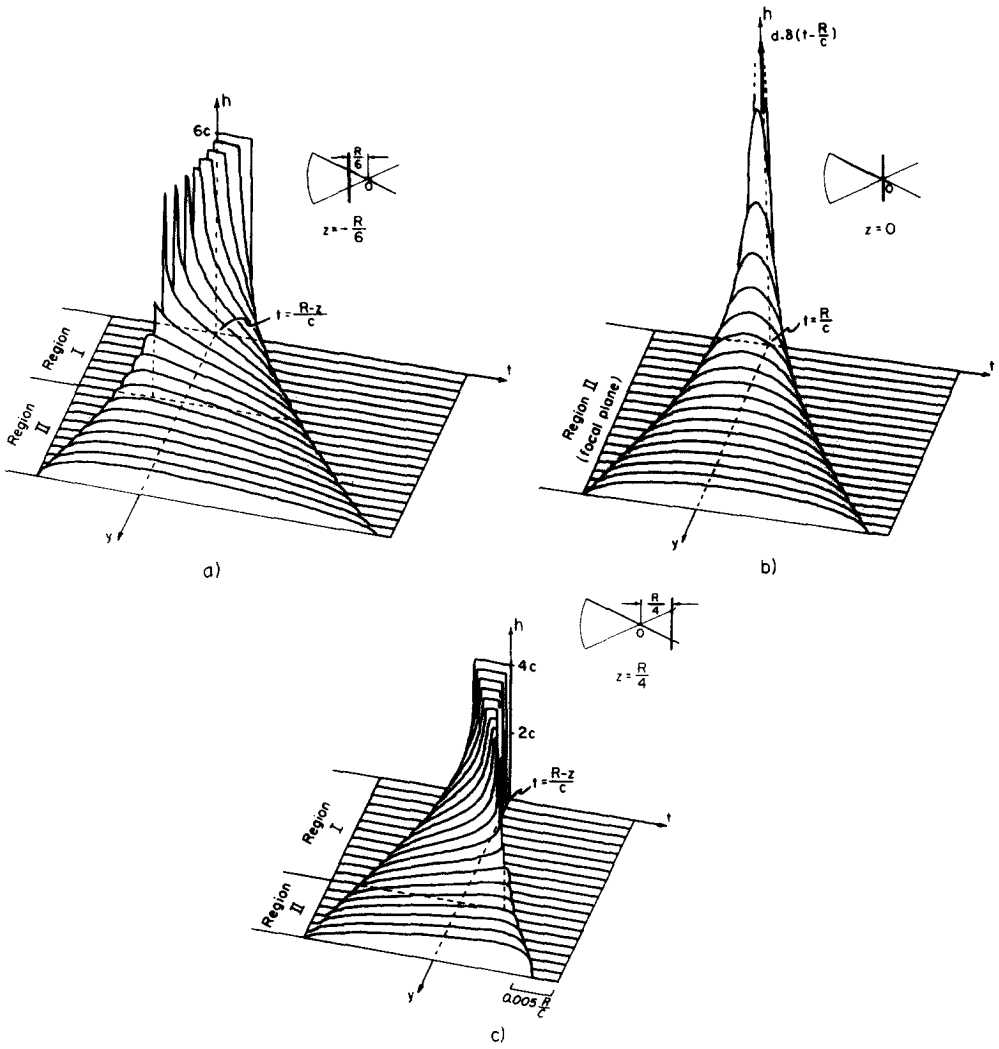

Fig. 4. Time dependence of the impulse response h of a focused radiator with R/a = 4.8, at three depths a) z = -R/6, b) z = 0 and c) z = R/4. In each case, the origin of the t-axis is set at the arrival time (R-z)/c from the center of the radiator to the axial position (y=0,z). Note the change in behaviour at the transition between Region I and II, as well as the convergence to a δ-function at the center of curvature.

expression because of the number of cases to consider, a computer treatment of Eq. (13) is quite straightforward. Figure 6 illustrates the decomposition of the impulse response h_a into its two components h_1 and h_2, at three off-axis positions in the field of a focused annular aperture with a) z = -R/6, b) z= 0, and c) z = R/4. The off-axis position y in each case was equal to $a_2/4\sqrt{2}$, while the annulus parameters were $R/a_2 = 4.8$ and $a_1 = a_2/4\sqrt{2}$. Note the new breakpoints introduced by the subtraction of h_1 from h_2, and the characteristic "canoe-like" shape of h_a in the focal plane.

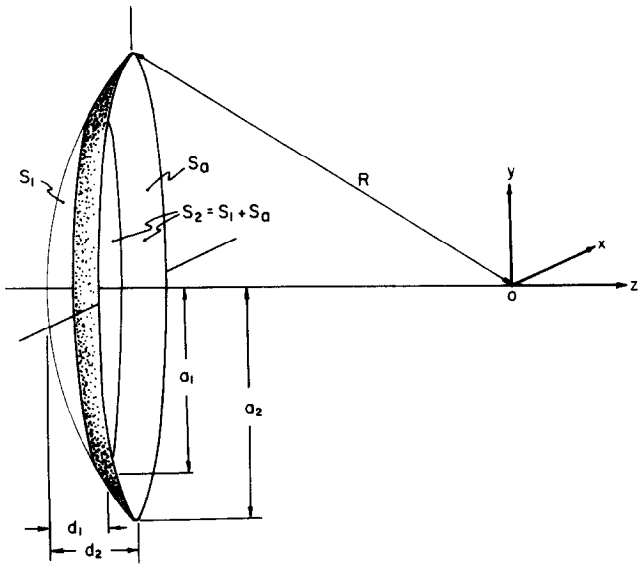

Fig. 5. Geometry of single concave annulus. Its surface S_a (only the outer side is shaded) is considered as the difference between the spherical shells S_1 and S_2.

c) Concave, phased annular arrays

The above description of the annular impulse response can now be applied to the case of phased annular arrays. The impulse response of electronically focused plane annular arrays has been discussed in detail by Dietz et al. [18]. These authors studied the focal plane response of an aperture consisting of a central piston and several concentric annuli, the array being electronically focused by compensating for the path differences between the elements and the focus. Their model further assumed that the plane of observation was in the far field of the array elements, and treated the annular elements as being infinitely thin.

The theory presented here applies to the case of concave annular arrays without the above restrictions. The advantages of the focused geometry in a practical imaging system have been discussed by Ueda et al. [15]. To focus an array with radius of curvature R at a depth f, the time delay Δt_j, between the j-th element of radius a_j and the centre of the array is approximately given by

$$\Delta t_j = \frac{a_j^2 \left(\frac{1}{R} - \frac{1}{f} \right)}{2\,c} \quad . \tag{14}$$

The above expression is accurate enough for most practical purposes where the radius of the outer annulus a_N satisfies $(a_N/f)^2 << 1$ for all f considered. The quantities a_j in Eq. (14) are the effective element

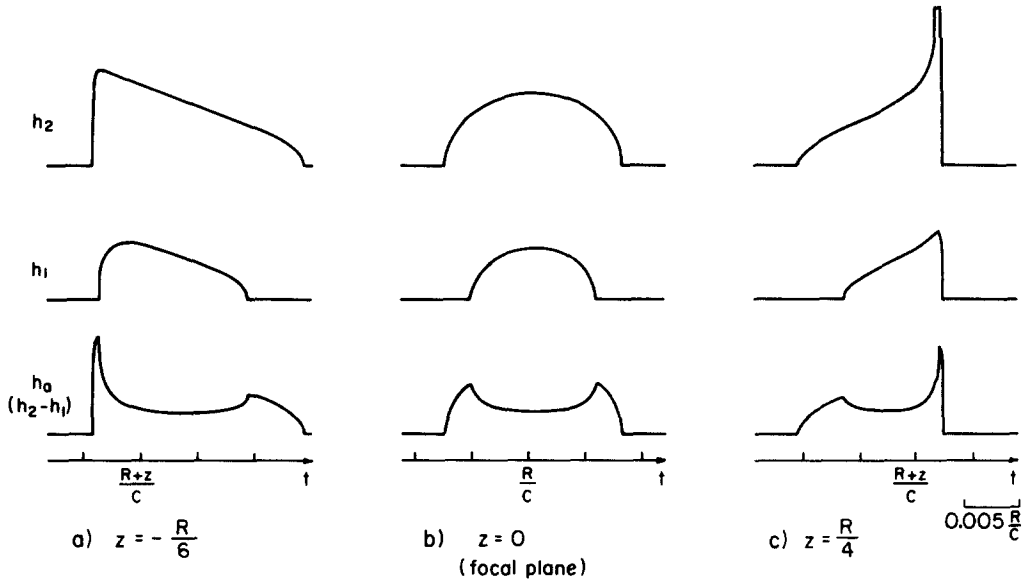

Fig. 6. Relative amplitude of typical off-axis impulse responses h_a of a spherically curved annulus, with their two components h_2 and h_1. The annulus parameters are $R/a_2 = 4.8$ and $a_1 = a_2/\sqrt{2}$. Three positions are examined: a) in front of, b) at, and c) behind the focal plane, with $y = a_2/4\sqrt{2}$ in each case.

radii corresponding to the mean path length to the j-th element, and are approximately given by

$$a_j = \{ (a_{j_1}^2 + a_{j_2}^2) / 2 \}^{1/2} \quad , \tag{15}$$

where a_{j_1} and a_{j_2} are the inner and outer radii of the j-th element. Note that since Δt_j is proportional to the square of a_j, array elements of equal areas have an equal phase shift across their radial width for all focal lengths. The spherical geometry (or the use of an acoustic lens with a plane annular array) allows the minimization of the maximum time delays required. This is achieved when R is set by

$$\frac{1}{R} = \frac{1}{2} \left(\frac{1}{f_1} + \frac{1}{f_2} \right) \quad , \tag{16}$$

with f_1 and f_2 being the shortest and longest focal depths considered, respectively.

The resultant impulse response of an array of N equally weighted annular elements with time delays Δt_j can be expressed analytically as

$$h(\vec{r},t) = \sum_{j=1}^{N} h_{a_j}(\vec{r},t-\Delta t_j) \quad , \tag{17}$$

where h_{a_j} is the impulse response of the j-th annulus, as given by Eq. (13). If desired, the individual h_{a_j} may be weighted in Eq. (17) to simulate apodization or Fresnel focusing of the array [22]. In the pulse-echo operation of a phased array, different elements might be used to transmit and receive. When this is the case, separate impulse responses are calculated for each mode and convolved as explained by Dietz et al. [18] and Foster et al. [23] to give the overall response.

It is interesting at this point to examine graphically the effect of the delay pattern given by Eq. (14) on the build-up of the impulse response of an electronically focused annular array. Figure 7 illustrates the summation process in Eq. (17) for the case of a focused aperture divided into five elements of equal areas. In this example, the center element and the four annuli are not separated by gaps and completely fill the aperture. The ratio of the radius of curvature R to the outer radius a of the array (R/a) is 4.8, and the off-axis position for all cases examined is given by $y = a/4\sqrt{2}$.

Figure 7(a) shows the off-axis impulse response of the array at two depths in the field: z = 0 (geometric focal plane) and z = -R/6 (see inset). No delays are considered in this case, and the array is thus focused at its center of curvature. The individual impulse responses of the annuli for z = 0 have the characteristic "canoe-like" shape, which, when summed with that of the center element, give the exact impulse response of the complete aperture. Similarly, the summation of the individual responses for z = -R/6 yields the impulse response characteristic of the complete aperture at this off-focal plane position.

The same field points are considered in figure 7(b). However here, delays Δt_j are imposed to the individual responses according to Eq. (14) to simulate electronic focusing of the array at z = -R/6 (i.e. f = 5/6 R). The summations of the delayed impulse responses at both field points now approximate those achieved by a single solid aperture of same outside diameter focused at 5/6 R, shown for comparison as dashed lines. The position at z = -R/6 lies now in the "electronic" focal plane of the array, whereas the array response at z = 0 (geometric focal plane) appears, by contrast, characteristic of an off-focal plane response: the focus has been effectively shifted to z = -R/6.

In a similar way, figures 7(c) and 7(d) illustrate impulse responses for geometric and electronic focusing of the array, this time placing the observation points at z = 0 and z = R/4 (see insets). By setting the electronic focal length at f = 5/4 R, the array responses approximate those of a solid aperture, focused at the depth f (dashed lines), indicating an effective focus shift to the plane z = R/4. Note that, from Eq. (14), the delays Δt_j needed for f = 4/5 R were equal and opposite to those for f= 6/5 R.

The discrepancies between the impulse responses of the electronically focused annular array and those of the solid apertures

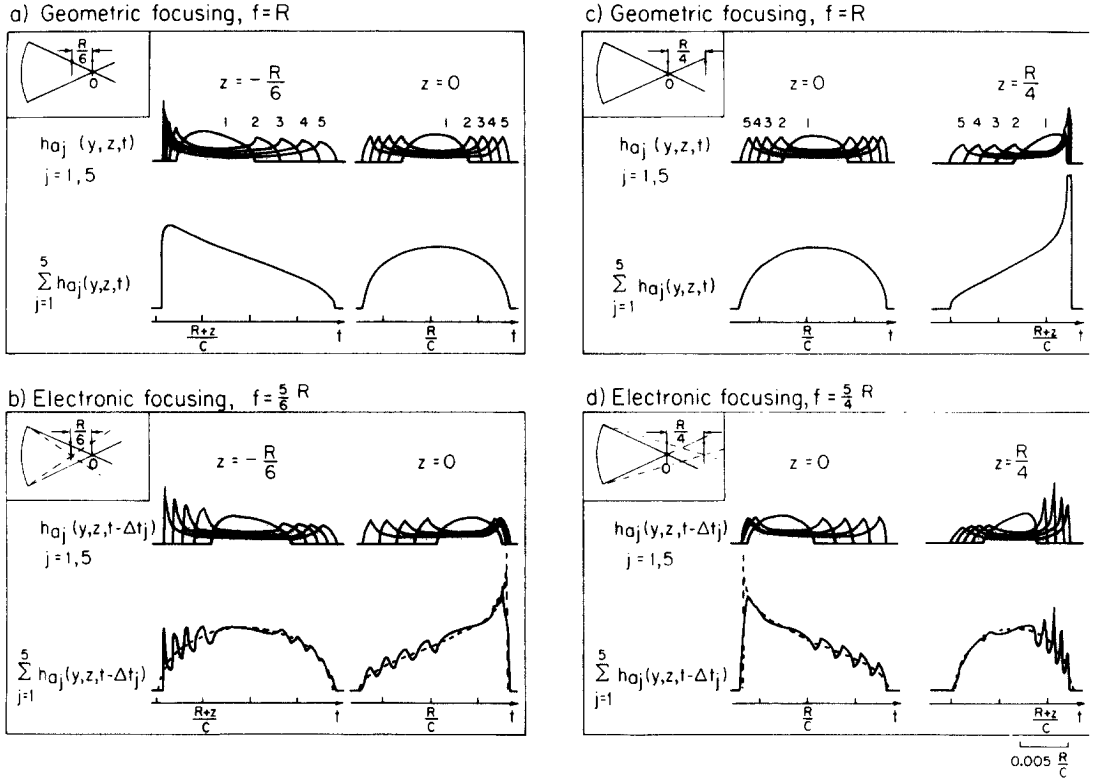

Fig. 7. Relative impulse responses of a phased, five element annular array. Starting with the centre element, the individual responses are numbered 1 to 5. The five elements have equal areas and completely fill the aperture. The outer element radius a is such that R/a = 4.8, and the observation points are the same as in figure 6 ($y = a/4\sqrt{2}$, z given in insets).

a) The impulse responses h_{aj} of the array elements as well as the total array response are shown at the two depths z = 0 and z = -R/6.

b) The individual h_{aj} are delayed by Δt_j to simulate electronic focusing of the array with f = 5/6 R. Their sums now approximate the impulse responses of a single solid aperture focused at z = -R/6 (dashed lines).

c) and d) Same as a) and b), but for the array electronically focused at z = R/4.

depend on: 1) the number of elements and 2) the widths of the gaps between elements. It is clear that as the number of annuli increases, improved agreement is achieved. Although the forgoing discussion assumed gaps of zero width, the effects of gap size on the array response are easily studied using Eq. (17), which sets no restrictions on the relative widths or spacing of the annuli.

IV. PRESSURE DISTRIBUTIONS

In this section, we describe how the technique presented above can be used in practice to calculate pressure fields. Equation (5) gave the general relationship between the impulse response of a given source geometry and the instantaneous pressure field, in terms of a convolution product with a particular excitation function. Analytic solutions for the pressure distributions of a focused radiator exist only for a few special cw cases. In Appendix B, we examine the cw pressure distributions on the axis and in the focal plane of a solid apeture. Our results, derived by means of the Fourier transform of h, are identical to those obtained differently by O'Neil [3]. In the case of pulsed annular arrays, the convolution integral of Eq. (5) must be computed numerically. When the particle velocity at the face of the radiator is non-zero over a short time interval (short pulse), its Fourier spectrum extends over a wide range of frequencies. In this case, the integration of Eq. (5) is most efficiently performed by direct numerical convolution, rather than by spectral analysis. The sampling of the functions to be convolved is of critical importance and will be discussed in detail.

a) Computational Method

The first term in Eq. (5) is the excitation function $\partial v_0/\partial t$, which is independent of the observation point. Note that $v_0(t)$ represents the particle velocity at the face of the source and thus includes the transducer's electromechanical response. The function $\partial v_0/\partial t$ may be directly measured with a small, wideband hydrophone positioned at the geometric focus. As noted previously, the pressure waveform at this point is a scaled replica of the excitation function. Alternatively, a model pulse may be used to simulate the excitation function.

The second term of the convolution integral in Eq. (5) is the impulse response $h(\vec{r},t)$. In order to perform the numerical integration, the analytic expressions described in Section III are sampled at the same rate as the excitation waveform. Unfortunately, the discontinuities and breakpoints characteristic of h complicate this procedure. While a sampling rate of about 10 times the highest frequency component of the excitation function leads to an accurate reproduction of the waveform, the same rate is in many cases insufficient for sampling $h(\vec{r},t)$, because of its sudden slope changes. As Lockwood and Willette noted for the case of a plane piston [7], the problem is particularly severe for observation points close to the boundary of the geometric projection of the source. We found that this is also true for focused apertures. The solution we have adopted consists of calculating the average value of the impulse response within each sampling interval T used for the excitation function. The number of values being averaged was proportional to the largest slope in each interval. Typically, we used one value per interval in the constant portions of $h(\vec{r},t)$, and up to 30 values per interval near the breakpoints. The average was then stored as one sample, ready to be convolved with the excitation function. In this manner, we obtained consistant results with good accuracy ($\sim$1%) without requiring an excessive number of samples to be convolved.

A second question of importance in the sampling of $h(\vec{r},t)$ is that of normalization, because the center of curvature is a singularity of this function. We have mentioned earlier (Eq. 12) that, at this point, $h(\vec{r},t)$ is a δ-function. Therefore, according to the sampling algorithm described above, the unique sample in this case is the integral of $h(\vec{r},t)$ over the interval T centered at the time R/c. From Eq. (14) and the

definition of the δ-function, the value to be stored for the centre of curvature is simply the depth d of the concave radiator. For the other points, the value of the i-th sample h^i is given by

$$h^i = \bar{h}^i \quad T \quad , \tag{18}$$

where $\bar{h}^i$ is the average of $h(\vec{r},t)$ within the i-th time interval.

b) Example

To illustrate the above discussion, we consider a practical case of pressure distribution from a pulsed annular array. We have developed a set of versatile computer programs, allowing beam profile calculations for various source geometries. In this example, the source is a five element annular array with a radius of curvature R of 12 cm and an outer diameter of 5 cm. Its five elements have equal areas and completely fill the aperture. The excitation function was a simulated 4 MHz model pulse, shown with its frequency spectrum in figure 8. The waveform was sampled at 100 MHz. Three perspective plots are given in figure 9, showing peak pressure profiles in water for the following cases: a) electronic focusing, as described in Section III, at a depth f = 5/6 R = 10 cm; b) geometric focusing of the array (no delays); and c) electronic focusing at a depth f = 5/4 R = 15 cm. The shifting of the limited geometric focal area is clearly illustrated in this figure. Because the aperture is kept the same in all cases, the effective f-number (focal length f/aperture diameter) of the array increases with the focal length. The full width at half maximum of the beam is 1.1, 1.3 and 1.6 mm at the three focal depths, corresponding to f-numbers of f/2, f/2.4 and f/3, respectively. The array beam widths are within 3 percent of the expected values from diffraction theory, calculated at the pulse mean frequency for solid apertures with comparable parameters.

The pressure distributions given as examples illustrate a practical use of the analytic treatment of the annular array impulse response. The array parameters were chosen to produce beam characteristics close to the diffraction limit. Theoretical focusing studies can be carried out in a similar manner for the pulse-echo operation of the array, and target or receiver responses may be easily incorporated in the analysis.

V. SUMMARY AND CONCLUSIONS

The ability to predict the focusing properties of ultrasonic radiators plays a vital role in the design of new ultrasonic imaging systems. In the case of a pulsed radiator, the impulse response approach provides the most efficient and accurate means of obtaining this information. We have derived a new formulation for the impulse response of a concave radiator and have examined the application of this analytic solution to predict the pressure fields of pulsed annular arrays.

The total impulse response of a phased annular array was treated as the sum of the delayed impulse responses of the individual annuli. As an example, the impulse response of a five element annular array was examined at various positions in the field of the transducer. Simulating electronic focusing, the action of the delays served to synthesize an impulse response approximating that of a focused solid aperture. The performance of the array depends on the accuracy of this approximation which is affected by the number, width, and spacing of the annuli. Our formulation is particularly useful for examining the effects of these

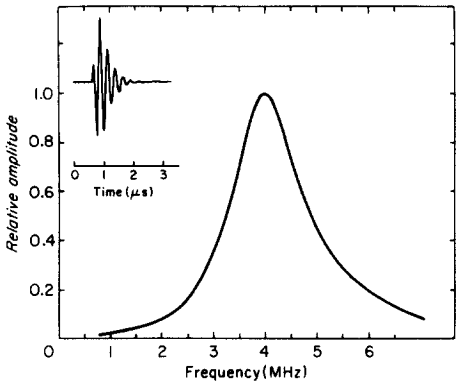

Fig. 8. Simulated 4 MHz model pulse with its frequency spectrum.

variables in a particular application, since no restrictions are imposed on the dimensions or spacings of the annuli.

Once the impulse response has been obtained, the pressure distribution may be determined by simple numerical convolution with the excitation function of the transducer. As an example, we considered a five element, f/2.4, annular array. The geometric focus was at 12 cm, and three-dimensional pressure distributions were given for electronic focal lengths of 10, 12, and 15 cm. These parameters correspond to the examples given in Section III. The results showed that, even with such a small number of annuli, the focal beam widths were within 3 percent of the theoretical diffraction limit.

From our experience, the computer programs based on the analytic impulse response have proven to be invaluable tools in the design of focused annular arrays. They provide a means for examining not only beam width but also depth of field, off-focal plane response and side-lobe structure of strongly focused arrays.

ACKNOWLEDGEMENTS

We would like to thank the National Cancer Institute of Canada and the Ontario Cancer Treatment and Research Foundation for supporting the work presented in this paper. One of the authors (M.A.) expresses his gratitude to the company Ebauches-SA, Neuchâtel, Switzerland, and to the Fonds National Suisse pour la Recherche Scientifique, Berne, Switzerland, for their financial support.

APPENDIX A: DERIVATION OF THE IMPULSE RESPONSE OF SPHERICALLY CURVED RADIATORS

This appendix gives a detailed derivation of the analytic expression for the impulse response of spherically curved radiators, given in

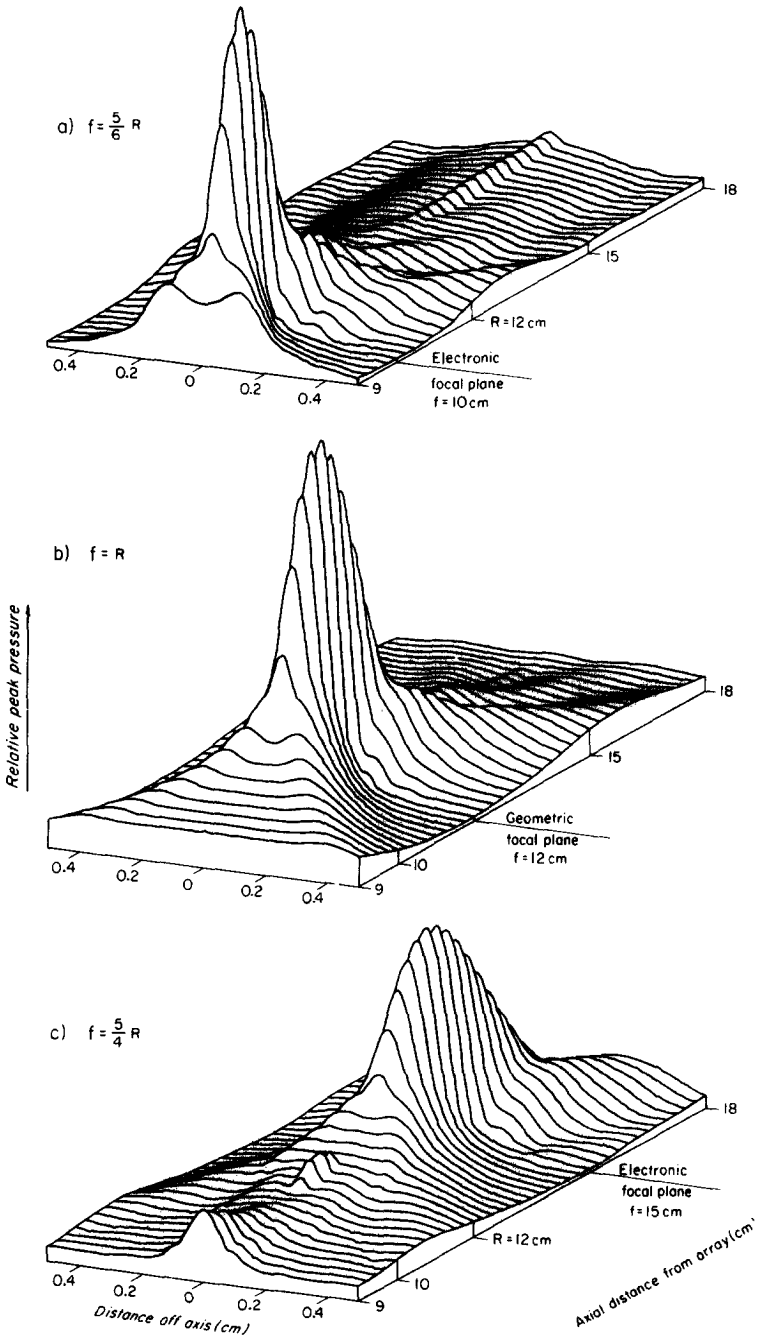

Fig. 9. Relative peak pressure distributions from a five element array similar to that described for figure 7: its 12 cm radius of curvature and 5 cm diameter define an f-number of f/2.4 at the geometric focal plane, while electronic focusing of the array at 10 cm and 15 cm corresponds to f/2 and f/3, respectively. The excitation function is shown in figure 8.

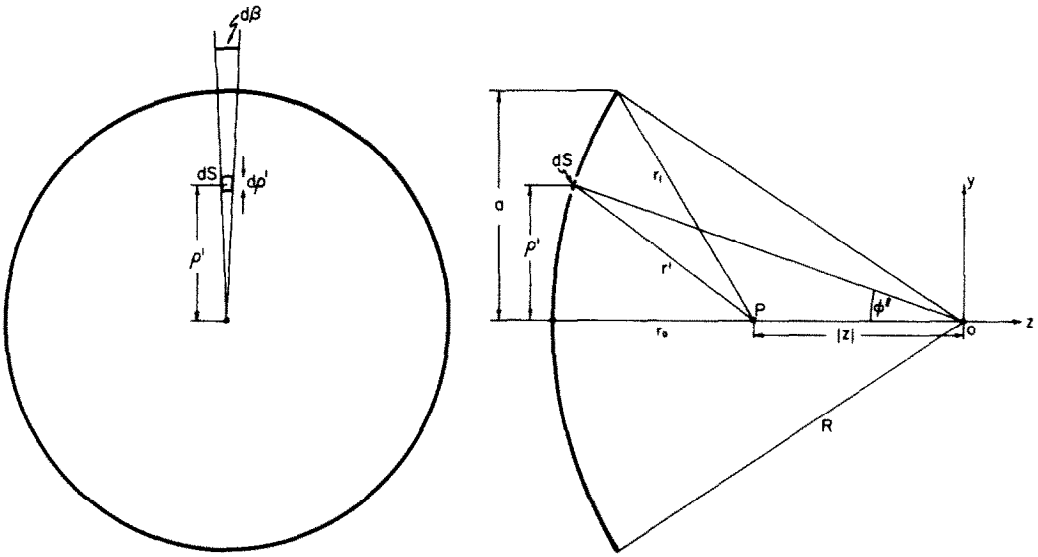

Fig. A-1. Geometry for the evaluation of Eq. (A1) with P on the axis of symmetry. In this case, $r=|z|$.

a) Front view of the radiator's surface;
b) Projection in the (y,z) plane.

table I. According to the definition of the impulse response, we wish to evaluate

$$h(\vec{r},t) = \frac{1}{2\pi} \int_S \frac{\delta(t - r'/c)}{r'} \, dS \qquad (A1)$$

over the surface S of the radiator, for field points $P(\vec{r})$ in both Regions I and II shown in figure 2. Before deriving the general solution, we first consider the on-axis case.

i) On-axis case

To evaluate Eq. (A1), ρ' is defined as the distance from the z-axis to the integration element dS, ϕ' is the angle subtended by the center of the radiator and dS at the origin, and $d\beta$ is the incremental angle bounding dS (see Fig. A-1). One has

$$dS = \frac{\rho' d\rho'}{\cos \phi'} \, d\beta = \frac{R}{|z|} r' \, dr' \, d\beta \quad . \qquad (A2)$$

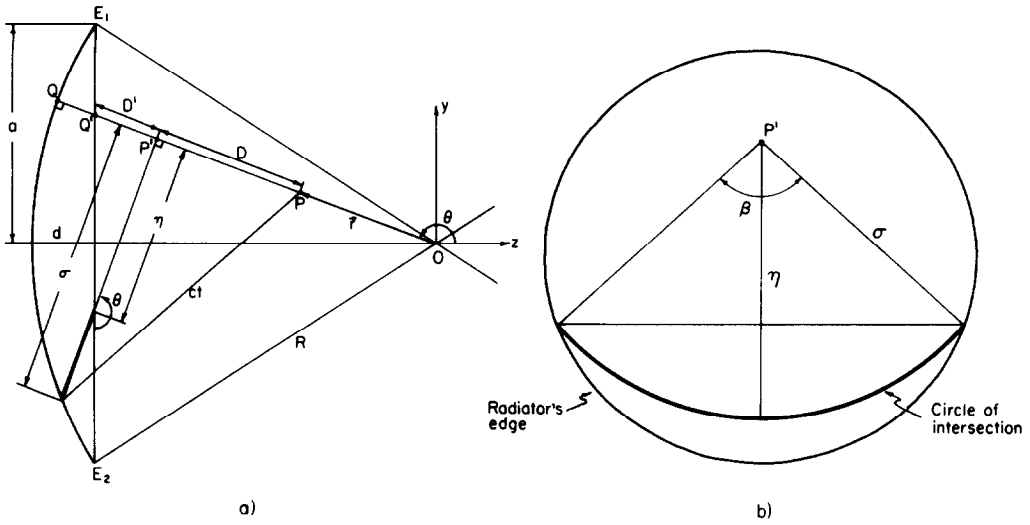

Fig. A-2. Geometry for the evaluation of the off-axis impulse response.

a) The thick line is the projection on the (y,z) plane of the intersection between the source and a sphere of radius ct centered at P.

b) This diagram shows the quantities η and σ in the plane of the circular intersection, centered at P'.

Substituting Eq. (A2) into Eq. (A1) then gives:

$$h(z,t) = \frac{1}{2\pi} \int_0^{2\pi} \int_{r_i}^{r_j} \frac{\delta(t - r'/c)}{r'} \frac{R}{|z|} r' \, dr' \, d\beta \qquad \text{(A3)}$$

or, because $\delta(t)$ is a function of time:

$$h(z,t) = \frac{c\,R}{|z|} \int_{r_i/c}^{r_j/c} \delta(t - r'/c) \, d\left(\frac{r'}{c}\right) \qquad \text{(A4)}$$

where we have used,

$$\text{for } z < 0 \begin{cases} r_i = r_o \\ r_j = r_1 \end{cases} \quad \text{and for } z > 0 \begin{cases} r_i = r_1 \\ r_j = r_o \end{cases} \tag{A5}$$

with r_o and r_1 defined in figure A-1.

Because of the definition the δ-function, the integral in Eq. (A4) is equal to unity for times t included in the integration interval, and identically zero outside the interval. The axial impulse response is thus:

$$h(z,t) = \begin{cases} \dfrac{c\,R}{|z|} & \text{for } r_i < ct < r_j \\ 0 & \text{otherwise .} \end{cases} \tag{A6}$$

Physically, this means that if a velocity impulse is applied at the face of the spherical radiator at time zero, the velocity potential at P jumps to a constant value after the arrival of the contribution from the closest region of the radiator (the center for $z < 0$, the edge for $z > 0$) and suddenly returns to zero after the arrival of the last contribution from the source.

ii) Off-axis case

To simplify the discussion, we shall consider the point P inside Region I with $z < 0$. In this case, we have $r_o < r_1 < r_2$ (Fig. 3(a)). Between the time r_o/c and r_1/c , in other words before the first arrival from the closest edge E_1, the on-axis derivation can be applied when one considers the axial symmetry around the line OPQ (Fig. A-2(a)). Here, for $t < r_1/c$, $h(\vec{r},t)$ becomes:

$$h(\vec{r},t) = \begin{cases} 0 & \text{for } ct < r_o \\ \dfrac{c\,R}{|\vec{r}|} & \text{for } r_o < ct < r_1 \text{ .} \end{cases} \tag{A7}$$

In the time interval between the arrivals from the edges E_1 and E_2, the axial symmetry no longer exists. From the definition of the impulse response, one now has

$$h(\vec{r},t) = \frac{c\,R}{r}\,\frac{1}{2\pi} \int_0^{\beta(t)} d\beta \int_{r_1/c}^{r_2/c} \delta(t - r'/c)\; d\left(\frac{r'}{c}\right) \tag{A8}$$

or:

$$h(\vec{r},t) = \begin{cases} \dfrac{c\,R}{r}\,\dfrac{\beta(t)}{2\pi} & \text{for } r_1 < ct < r_2 \\ 0 & \text{for } r_2 < ct \end{cases} , \tag{A9}$$

where the angle $\beta(t)$, illustrated in figure A-2(b), subtends the arc length of points on the radiator equidistant from P. This angle $\beta(t)$ determines the time dependence of h in its variable portion.

Bearing this in mind, $\beta(t)$ may be determined from the intersection of the spherical radiator with a sphere of radius ct centered at P. Figure A-3 is given to help the reader visualize this intersection (thick line) in relation to the other quantities used in figure A-2. The intersection, for $t > r_1/c$ is not a complete circle but an arc subtended by $\beta(t)$ centered at P'. In the plane of the intersection, $\beta(t)$ may be evaluated and is given by

$$\beta(t) = 2\cos^{-1}\left(\frac{\eta(t)}{\sigma(t)}\right) , \tag{A10}$$

where η and σ are defined in figure A-2(b). The time dependence of these quantitites may be determined in the (y,z) plane. Using the quantity D defined in figure A-2(a) and the two relationships

$$R^2 = (r + D)^2 + \sigma^2 \tag{A11}$$

$$c^2t^2 = D^2 + \sigma^2 , \tag{A12}$$

we obtain:

$$\sigma(t) = R\left[1 - \left(\frac{R^2 + r^2 - c^2t^2}{2rR}\right)^2\right]^{1/2} \tag{A13}$$

and

$$D = \frac{R^2 + r^2 - c^2t^2}{2\,r} - r . \tag{A14}$$

Now η is obtained from the relationship

$$\eta = \frac{-D'}{\tan\theta} , \tag{A15}$$

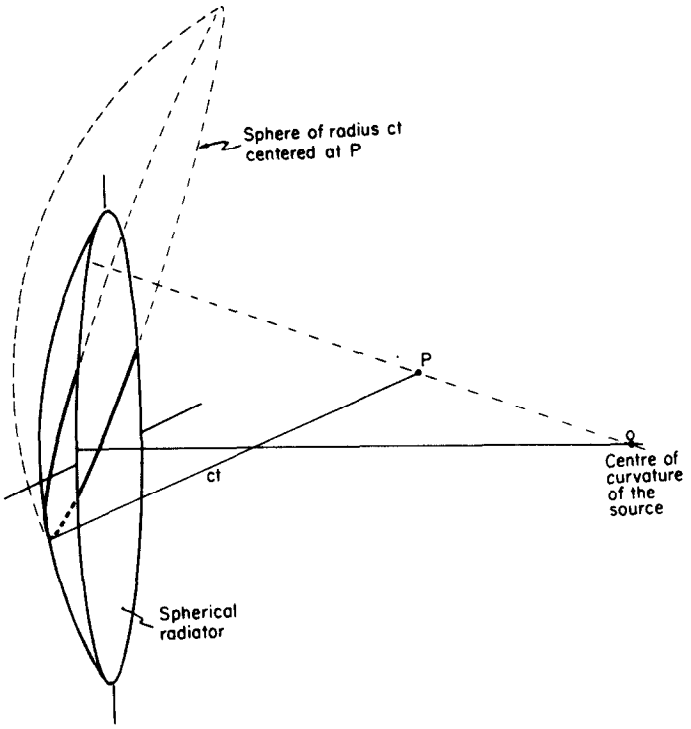

Fig. A-3. Perspective view of the intersection between the spherical source and the sphere of radius ct centered at P.

where D', defined in figure A-2(a), is given by:

$$D' = - \frac{R - d}{\cos \theta} - (D + r) \quad . \tag{A16}$$

Therefore, combining Eqs. (A14-A16) yields:

$$\eta(t) = R \left[\frac{1 - \frac{d}{R}}{\sin \theta} + \frac{1}{\tan \theta} \left(\frac{R^2 + r^2 - c^2t^2}{2rR} \right) \right] \quad . \tag{A17}$$

Substituting Eq. (A10) into Eq. (A9), we obtain for $t > r_1/c$:

$$h(\vec{r},t) = \begin{cases} \frac{c\,R}{r} \frac{1}{\pi} \cos^{-1}\left(\frac{\eta(t)}{\sigma(t)}\right) & \text{for } r_1 < ct < r_2 \\ 0 & \text{for } r_2 < ct \quad . \end{cases} \tag{A18}$$

where $\eta(t)$ and $\sigma(t)$ are given by Eq. (A17) and Eq. (A13), respectively.

This completes the derivation of $h(\vec{r},t)$ for the Region I with $z < 0$.

It may be shown that Eqs. (A13) and (A17) are also valid for field points in Region I with $z > 0$, and in Region II. The remainder of the equations in table I may be derived on the basis of the above equations to give a complete picture of the impulse response in the field of a spherical radiator.

APPENDIX B: CW PRESSURE DISTRIBUTIONS

Here, we examine how cw pressure distributions from a focused aperture can be derived using the impulse response given in table I. In the cw case, Eq. (5) must be rewritten in a more explicit form. For this purpose, we write the excitation velocity at the face of the source as

$$v_o(t) = u_o e^{j\omega_o t} \tag{B1}$$

where ω_o is the driving angular frequency, and u_o the velocity amplitude. Therefore, Eq. (5) may be expressed as

$$p(\vec{r},t) = -j \rho u_o \omega_o \int_{-\infty}^{\infty} e^{j\omega_o(t - t')} h(\vec{r},t') \, dt' \quad , \tag{B2}$$

where the integral now represents the Fourier transform of $h(\vec{r},t)$.

As Lockwood and Willette [7] noted, the cw pressure amplitude can thus be derived from the impulse response by a single numerical integration of Eq. (B2) over the interval of definition of the nonzero part of $h(\vec{r},t)$ evaluated at the driving frequency ω_o. These authors reported excellent results, obtained numerically for the impulse responses of circular and rectangular plane radiators. For spherically curved radiators, two particular cases lend themselves to an analytic treatment: The on-axis and the focal plane responses.

The axial distribution is found by substituting Eq. (11) into Eq. (B2), which yields

$$p(z,t) = -j\rho u_o \omega_o e^{j\omega_o t} \frac{c\,R}{|z|} \int_{-\infty}^{\infty} e^{-j\omega_o t'} \operatorname{rect}\left(\frac{t' - M/c}{\Delta(z)/c}\right) dt' \, . \tag{B3}$$

This integral is easily evaluated and leads to O'Neils's expression for the cw axial pressure [3]:

$$p(z,t) = j\rho c u_o \frac{2\,R}{z} \sin\left(\frac{\omega_o}{c}\frac{\Delta(z)}{2}\right) e^{j\omega_o(t - M/c)} \, . \tag{B4}$$

Another analytic solution exists for the cw pressure distribution in the focal plane of the spherical radiator. However in this case, several approximations are required. From Eq. (B2), we see that the solution is proportional to the Fourier transform of the focal impulse response. Recalling the expressions of table I, and noting that in the focal plane,

$$\theta = 90^{o} \quad , \quad \frac{1}{\tan \theta} = 0 \quad \text{and} \quad |\vec{r}| = y \quad , \tag{B5}$$

the impulse response becomes

$$h(\vec{r},t) = \begin{cases} 0 & \text{for} \quad ct < r_1 \\ \dfrac{c\,R}{\pi\, y} \cos^{-1}\left(\dfrac{1 - \dfrac{a^2}{2\,R^2}}{\left[1 - \dfrac{R^2}{y^2}\left(1 + \dfrac{y^2}{R^2} - \dfrac{c^2t^2}{R^2} \right)^2 \right]^{1/2}} \right) & r_1 < ct < r_2 \\ 0 & r_2 < ct \quad . \end{cases} \tag{B6}$$

Provided that the point of observation satisfies $y^2/R^2 << 1$, and using the definition

$$\tau \equiv \frac{1}{c} \left(R^2 + y^2 \right)^{1/2} \quad , \tag{B7}$$

the non-zero part of Eq. (B6) is approximated by its second-order Taylor's expansion as

$$h(y,t) \simeq \frac{c\,R}{y} \frac{1}{\pi} \cos^{-1}\left[\left(1 - \frac{a^2}{R^2} \right) \left(1 + \frac{c^2(t - \tau)^2}{2\,y^2} \right) \right] . \tag{B8}$$

With the additional provision that the radius of the source satisfies $a^2/R^2 << 1$, Eq. (B8) can be simplified to

$$h(y,t) \simeq \frac{c\,a}{\pi\, y} \left(1 - (t - \tau)^2\, \alpha^2 \right)^{1/2} \qquad \text{for} \quad r_1 < ct < r_2 \tag{B9}$$

with $\alpha \equiv cR/ay$. Substituting (B9) into (B2), the integral can be solved and yields the pressure distribution

$$p(y,t) = -j\rho u_o \omega_o\, e^{j\omega_o(t - \tau)} \frac{a^2}{2R} \left[\frac{2\, J_1\left(\dfrac{\omega_o a y}{cR} \right)}{\dfrac{\omega_o a y}{cR}} \right] \quad , \tag{B10}$$

where $J_1(x)$ is the first order Bessel function of the first kind. Therefore, when the radius of the source is small compared to its radius of curvature, and when the point of observation is close to the axis, the focal plane pressure distribution is approximately given by the well-known Airy pattern. Note that rather severe restrictions were imposed in order to obtain this result. The analytic form of the impulse response given in table I is more general, and is therefore capable of providing more accurate pressure distributions, over a wider range of field points.

REFERENCES

[1] Gruetzmacher, J., Piezoelektrischer Kristall mit Ultraschallkonvergenz, Zeits. f. Physik 96, 342-349 (1935).

[2] Labaw, L. W., Curved quartz crystals as supersonic generators, J. Acoust. Soc. Amer. 16, 237-245 (1945).

[3] O'Neil, H. T., Theory of focusing radiators, J. Acoust. Soc. Amer. 21, 516-526 (1949).

[4] Oberhettinger, F., On transient solutions of the "baffled piston" problem, J. Res. NBS, 65B, 1-6 (1961).

[5] Stepanishen, P. R., Transient radiation from pistons in an infinite planar baffle, J. Acoust. Soc. Amer. 49, 1629-1638 (1971).

[6] Stepanishen, P. R., The time dependent force and radiation impedance on a piston in a rigid infinite planar baffle, J. Acoust. Soc. Amer. 49, 941-849 (1971).

[7] Lockwood, J. C. and Willette, J. G., High-speed method for computing the exact solution for the pressure variations in the nearfield of a baffled piston, J. Acoust. Soc. Amer. 53, 735-741 (1973).

[8] Robinson, D. E., Lees, S., and Bess, L., Near field transient radiation patterns for circular pistons, IEEE Trans. Acoustics, Speech and Signal Processing ASSP-22, 395-403 (1974).

[9] Farn, C. L. S. and Huang, H., Transient acoustic fields generated by a body of arbitrary shape, J. Acoust. Soc. Amer. 43, 252-257 (1968).

[10] Freedman, A., Sound field of plane or gently curved pulsed radiators, J. Acoust. Soc. Amer. 48, 221-227 (1970).

[11] Kossoff, G., Design of narrow-beanwidth transducers, J. Acoust. Soc. Amer. 35, 905-912 (1963).

[12] Penttinen, A. and Luukkala, M., The impulse response and pressure nearfield of a curved ultrasonic radiator, J. Phys. D, 9, 1547-1557 (1976).

[13] Reid, J. M. and Wild, J. J., Current developments in ultrasonic equipment for mechanical diagnosis, Proc. Nat. Electronics Council 12, 44-58 (1956).

[14] Hubelbank, M. and Tretiak, O. J., Focused Ultrasonic Transducer Design, in Research Laboratory of Electronics, MIT, QPR 98, 169-177 (1970).

[15] Ueda, M., Sato, T., and Maeda, Y., Dynamic focusing ultrasonic transducer by using analog gate delay circuits, Bulletin of the Tokyo Institute of Technology 119, 55-63 (1973).

[16] Haverl, R. A., Stoller, M., Ultrasonic Body Scanner and Method, United States Patent #4,137,777, Mediscan Inc., Feb 6, 1979.

[17] Green, P. S., Havlice, J. F., Holzemer, J. F., Ramsey, S. D., Jr., Taenzer, J. C., and Moessner, H. Z., Design and construction of a dynamically focused annular array, IEEE Trans. Sonics and Ultrasonics, SU-25, 259 (1978).

[18] Dietz, D. R., Norton, S. J., and Linzer, M., Wideband Annular Array Response, in 1978 IEEE Ultrasonics Symposium Proceedings, pp 206-211 (IEEE Cat. 78CH 1344-1 SU).

[19] Dietz, D. R., Parks, S. I., and Linzer, M., Expanding-aperture annular array, Ultrasonic Imaging 1, 56-75 (1979).

[20] Strutt, J. W. (Lord Rayleigh), in Theory of Sound, Vol. 2 (Dover, NY, 1945).

[21] Goodman, J. W., in Introduction to Fourier Optics, p. 58 (McGraw-Hill, NY, 1969).

[22] Fink, M. and Larmande, T., Wideband Fresnel Focusing Array Response, 1979 IEEE Ultrasonics Symposium Proceedings, pp. 204-209 (IEEE Cat. 79CH 1482-9 SU).

[23] Foster, F. S., Patterson, M. S., Arditi, M., and Hunt, J. W., The conical scanner: A two transducer ultrasound scatter imaging technique, Ultrasonic Imaging 3, 62-82 (1981).